Electrical resistivity tomography array comparisons to detect cleared-wall foundations in brownfield sites

R. M. Eissa [1,2]*, N.J. Cassidy [1,3], J.K. Pringle [1] & I.G. Stimpson [1]

[1] *School of Geography, Geology and Environment, William Smith Building, Keele University, Staffordshire, ST5 5BG, UK.*

[2] *now Faculty of Engineering, Civil engineering department, University of Kerbala, Kerbala. Iraq.*

[3] *now School of Engineering, Civil engineering department, University of Birmingham, Birmingham, B15 2TT, UK.*

* *Corresponding author: (email: raad.m@uokerbala.edu.iq)*

Abstract

Electrical resistivity surveys are commonly used to detect and characterise near-surface buried objects in commercial developments of brownfield sites. 2D ERT profiles arrays predominate in such surveys due to their relatively rapid deployment, good penetration depths and fast data collection rates. However, there is a need to test the optimum array types in such surveys. A scaled-model was used to simulate a large cleared-building wall foundation in gravel-fill at a test facility, before multiple 2D ERT profiles were acquired using different array configurations. Results were used to generate 2D resistivity models using both least-square smoothness-constraint and robust inversion. 2D profile array comparisons showed that the Wenner and dipole-dipole arrays were the best in detecting the cleared-wall foundation, although dipole-dipole arrays better delineated the top of the wall foundation. This study suggests that both Wenner and dipole-dipole array configurations should be utilised to detect buried wall foundations for 2D resistivity surveys.

Keywords: near-surface geophysics, brownfield sites, electrical resistivity arrays, wall foundations, ERT, inversion.

Electrical resistivity surveys are common geophysical techniques that have been widely used for imaging the subsurface (Loke et al. 2013). The method has been applied, amongst other applications, for civil engineering, site investigation and characterisation studies (see, for example, Keary et al. 2002; Cosenza et al. 2006; al Hagrey and Petersen 2011; Reynolds 2011; Chrétien et al. 2014; Lysdahl et al. 2017; Long et al. 2017). Constant Separation Traversing (CST) electrical surveys are very commonly undertaken for archaeological (see Gaffney 2008; Gaffney et al. 2015) and forensic (Juerges et al. 2010) targets, rapidly covering a survey area, albeit at very shallow depths. In contrast, Electrical Resistivity Tomography (ERT) surveys are relatively slower to collect but can penetrate up to 150 m below ground level (see Keary et al. 2002; Zhu et al. 2017).

Researchers can use a variety of different ERT electrode configurations (termed arrays - see Szalai and Szarka 2008); Reynolds (2011) provides theoretical background for the different array types. Published case study examples include using pole-pole arrays to detect underground cavities (Garman and Purcell 2004), using pole-dipole arrays to characterise Karst bedrock (Nyquist and Roth 2005), Saad et al. (2010) used Wenner, Wenner-Schlumberger and pole-dipole arrays to detect voids, Banham and Pringle (2011) used Wenner arrays to detect coal mineshafts, Cuthbert et al. (2009) used Wenner array to study the superficial deposits architecture effects on groundwater recharge, and finally Cardarelli et al. (2010) used pole-dipole arrays to detect buried cavities.

Most ERT surveys in brownfield sites use 2D survey array configurations, due to their relatively rapid deployment and data collection speeds, usually after other geophysical surveys have approximately located target(s) positions (Reynolds 2011). Best practice

(Reynolds 2011) suggests that the buried target occurs along the plane of the survey line and in a perpendicular direction as others have suggested (Bentley and Gharibi 2004; Loke 2015). 3D ERT arrays are more time consuming to acquire, but produce more relevant results as resistivity variations will be in three dimensions. Resistivity data processing is also important, the collected data should be checked for consistency and quality, and routinely inverted by specialist software programmes to convert collected apparent to interpreted resistivity values (see Loke & Barker 1996; Loke & Dahlin 2002; Loke et al. 2003, 2007, 2010).

Several array comparisons studies have already been published. For example, Kampke (1999) compared the inversion process for linear arrays (Wenner alpha) for archaeological prospecting, and found that the focused imaging method could produce a good estimation of subsurface anomalies. Dahlin and Zhou (2004) compared several different array configurations on five synthetic datasets with anomalies present, using a least-square smoothness-constraint and robust inversions, and Stummer et al. (2004), Maurer et al. (2010) and Wilkinson et al. (2006/2012) compared optimised ERT survey designs. Results showed that pole-dipole, dipole-dipole, multiple gradient and Schlumberger arrays were recommended for 2D resistivity surveys, with array choice related to the geology, logistic issues and other site-specific variables.

For civil engineering purposes, resistivity surveys have been used to detect and characterise sites, for example, to determine subsurface characterization (Soupios et al. 2007), investigation of existing foundations (e.g. Cardarelli et al. 2007; Arjwech et al. 2013), or to monitor ground stabilisation procedures (e.g. Fischanger et al. 2013; Apuani et al. 2015). Resistivity imaging has been used for railway embankment conditions assessment (Donohue et al. 2011; Gunn et al. 2015). Moreover, ERT has been used for detecting natural (Deceuster et al., 2006; Zhu et al., 2011) and man-made (Chambers et al. 2007; Cardarelli et al. 2010; Orfanos and Apostolopoulos 2011) underground cavities as possible hazards that might be

effect civil construction integrity. Cardarelli et al. (2018) undertook 3D ERT surveys, as well as seismic tomographic surveys, to assess the conditions of an ancient Roman historical building. However, there has been little research to assess preferable 2D profile array configurations for detection and characterisation of cleared-wall foundations in brownfield sites.

More-sophisticated ERT interpretation methods use data inversion as a tool, to produce a 2D section of implied resistivity values from measured apparent resistivity data. The main aim of inversion theory is to produce an interpreted resistivity model of the sub-surface, that provides simulated apparent resistivity values that are a best match/fit to the collected data (see Loke and Barker 1995). The forward modelling programme generates simulated data, based on a finite-difference or finite-element method, and then the inversion technique is used to iteratively change the model until the simulated data matches the collected data (Dahlin 2001). The difference between simulated and collected data is measured and presented as root mean square (RMS) errors (see Loke and Dahlin 2002).

This paper aims to evaluate surface 2D ERT surveys to detect cleared-wall foundations in brownfield sites, and their appropriate survey parameters. Study objectives will therefore be to: (1) collect multiple 2D ERT datasets over a scaled model of a cleared-wall foundation in gravel-fill on a test site; (2) repeat the surveys using the four most commonly-used ERT array configurations (Wenner, dipole-dipole, pole-dipole, and pole-pole); (3) invert all datasets with the two commonly-used least-squares and robust methods and finally; (5) determine the best array type and inversion methods for 2D datasets.

97 **The test facility site**

98 The test site lies within the grounds of Keele University in Staffordshire, United Kingdom.
99 The bedrock geology is the late Carboniferous clastic sedimentary Butterton Sandstone Bed
100 of the Halesowen Formation at 1.2 m below ground level (bgl), with overlying Quaternary
101 glacial sandy soil deposits and water table depth at 3 m - 4 m bgl (Cassidy 2001).

102 A test pit, 0.8 m deep, 3 m long and 2.9 m wide, was excavated and a central
103 Victorian brick wall foundation built, 1.5 m long, 0.36 m wide and 0.48 m high, orientated in
104 an East-West direction (Fig. 1). The excavated sides were covered by an impermeable
105 membrane and drainage added before the wall was built. The pit was then back-filled with
106 clay-free, well-sorted, 4 mm quartz gravel and, with porosity of about 42%, to a depth of
107 ~0.55 m. The final ~0.25 m was refilled by re-cycled, compacted top soil and the test site
108 levelled (Cassidy 2001).

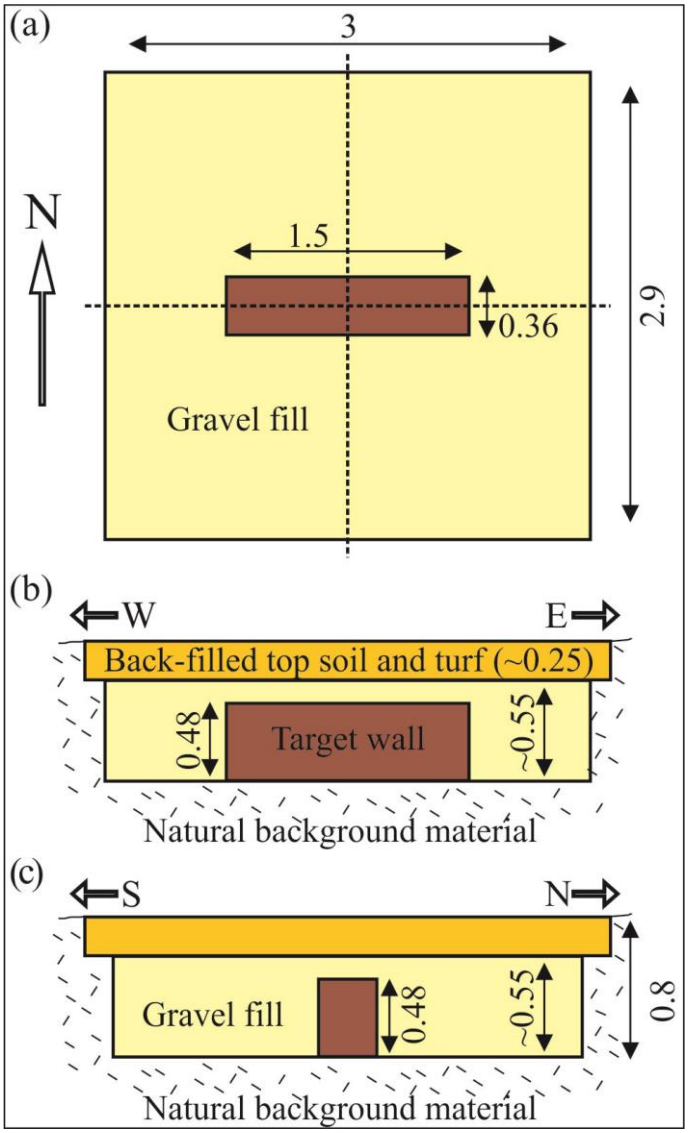

Figure 1: (**a**) plan view and (**b** & **c**) side views of the cleared buried wall foundation (brown), test site gravel infill and top soil fill (marked) within the test pit, with measurements in metres (adapted from Cassidy 2001).

Survey methodology and data processing

Two sets of ERT surveys were collected across the test site, over a period of 15 days, orientated north-south and east-west respectively (Fig. 2). Each survey consisted of three parallel 2D ERT profiles of 64 electrodes with 0.25 m electrode spacing (Fig. 2). The 16 m long ERT profile lengths were determined to gain sufficient penetration in the target area following initial trials. Repeat Wenner, pole-pole, dipole-dipole, and pole-dipole array ERT configurations (as well as repeats in both directions) were collected at each profile position (see Reynolds 2011 ch. 7 for more information).

In this study, the CAMPUS™ Tigre resistivity meter was used for data collection, using Imager™ pro 2006 v.1.1.4 controller software. Once the electrode probe contact resistances were checked for consistency for each profile, the meter was set to collect each reading with a 1 s duration and 3 cycles to gain an average. The number of resistivity data points and investigated resistivity levels were kept the same for each profile array for consistency purposes.

Within the N-S orientated ERT survey set, profile NS1 was located over the wall foundation centre, profile NS2 was located 0.75 m to the east of the foundation (at the wall-gravel interface) and profile NS3 was located 2.5 m to the east of the foundation (Fig. 2). Within the E-W orientated survey set, profile EW1 was located over the wall foundation centre, profiles EW2 and EW3 were located 0.75 m and 4 m to the north of the foundation respectively (Fig. 2).

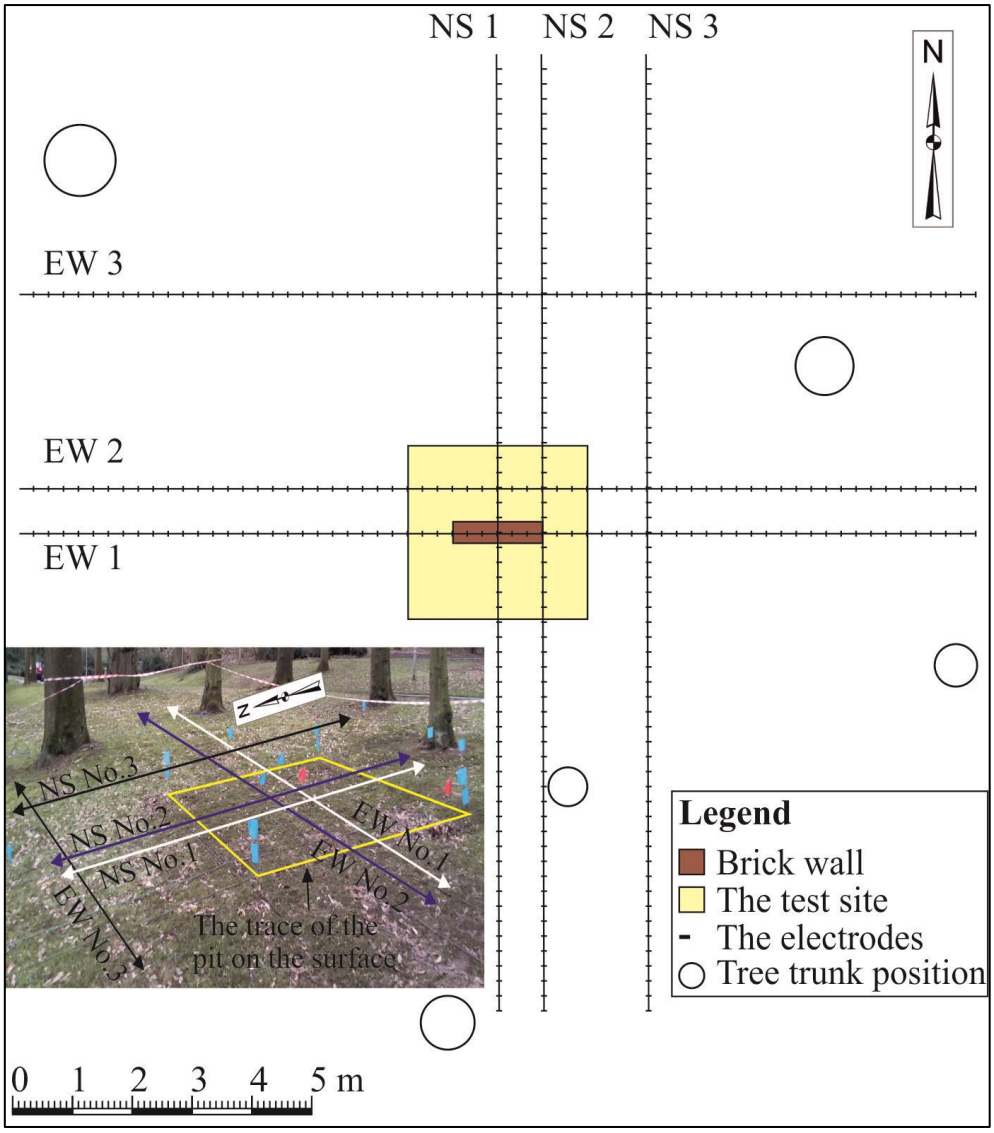

141

142 Figure 2: Schematic diagram showing the geophysical survey positions on the test site with
143 (inset) annotated photograph with survey profile locations indicated.

144

145

146 The resulting ERT datasets were initially checked for consistency and quality, with
147 anomalous data points (compared to adjacent measurements but considering target locations)
148 removed and adjacent measurements utilised to give an average value for removed points
149 using Surfer™ v.8.04 software. The number of collected and corrected data points are detailed
150 in Table 1. All resistivity surveys investigated deeper than the bottom of the cleared-wall
151 foundation, but the pole-pole data sets had a significant number of zero readings recorded,
152 therefore, just the target section was selected and processed to generate 2D resistivity models.

153 Note that the pole-dipole array configuration collects asymmetrical data (see Loke 2015), so
154 these data were collected on each survey profile in both directions, and the resulting pole-
155 dipole data merged to produce the respective images (Figs 3-4).

156 Table 1: Summary statistics of each ERT profile, array type, data points collected/inverted and
157 depth 'n' levels. Fig.2 for profile locations.

ERT Profile	Array	No. of collected data points	No. of corrected data points	Data 'n' levels
NS1	Wenner	600	7	15
	Dipole-dipole	873	0	18
	Pole-dipole	909	1	18
	Pole-pole	455	1	13
NS 2	Wenner	600	1	15
	Dipole-dipole	873	0	18
	Pole-dipole	909	0	18
	Pole-pole	455	1	13
NS 3	Wenner	600	20	15
	Dipole-dipole	873	72	18
	Pole-dipole	909	0	18
	Pole-pole	455	6	13
EW 1	Wenner	600	0	15
	Dipole-dipole	873	0	18
	Pole-dipole	909	0	18
	Pole-pole	455	3	13
EW 2	Wenner	600	2	15
	Dipole-dipole	873	13	18
	Pole-dipole	909	1	18
	Pole-pole	455	1	13
EW 3	Wenner	600	0	15
	Dipole-dipole	873	1	18
	Pole-dipole	909	1	18
	Pole-pole	455	2	13

158

159 Respective ERT array datasets were then finite-difference inverted within Geotomo™
160 Res2Dinv v.3.4 software, using first the non-linear, least-squares optimization algorithm
161 (using normal mesh and damping factors), and secondly using the robust inversion algorithms
162 (using respective 0.05 data and 0.01 model constrain cutoffs) for comparison (see Loke &
163 Barker 1996; Loke et al. 2007). The 5th model iteration and a common logarithmic, colour-
164 contoured interval was used throughout for consistency. The software set the depth of 'n'

level 1 at ~0.5 electrode spacing (a) for the Wenner, ~0.3a for dipole-dipole, 0.6a for pole-dipole and 0.9a for pole-pole array configurations respectively based on Edwards (1977).

Results

The 2D resistivity models (Figs. 3-6) showed obvious apparent resistivity contrasts between the test site gravel-fill materials and the natural ground, these materials having relatively high resistivity values (~2000 ohm.m or more) comparing to the background natural ground soil (~100-500 ohm.m). The brick wall foundation, compared to the gravel-fill volume, was less easily resolved in the 2D resistivity models (marked in Figs. 3-6), having relatively higher resistivity values (~3000 ohm.m or more), compared to the gravel-fill material. Based on the resistivity contrast between the natural background, the gravel-fill, the brick wall foundation, and the test site's dimensions (see Fig. 1), the resistivity models were then interpreted and compared.

The test site with gravel-fill material (annotated by the dotted white boxes on the 2D resistivity models – Figs. 3-6), had its spatial extent generally well imaged by all four array types, with the Wenner array better defining the test site edges and the dipole-dipole array better at defining the test site depth (Figs 3-4). The dipole-dipole and pole-dipole arrays were generally better at imaging the top of the buried wall foundation, whilst the Wenner and pole-pole arrays were better at imaging the bottom of the foundation (Figs 3-6); comparing with foundation's dimensions and position (*cf.* Figs. 3-6).

The thin top soil, of relatively lower resistivity, compared to the rest of the site, was well constrained and equally well defined in all array configurations.

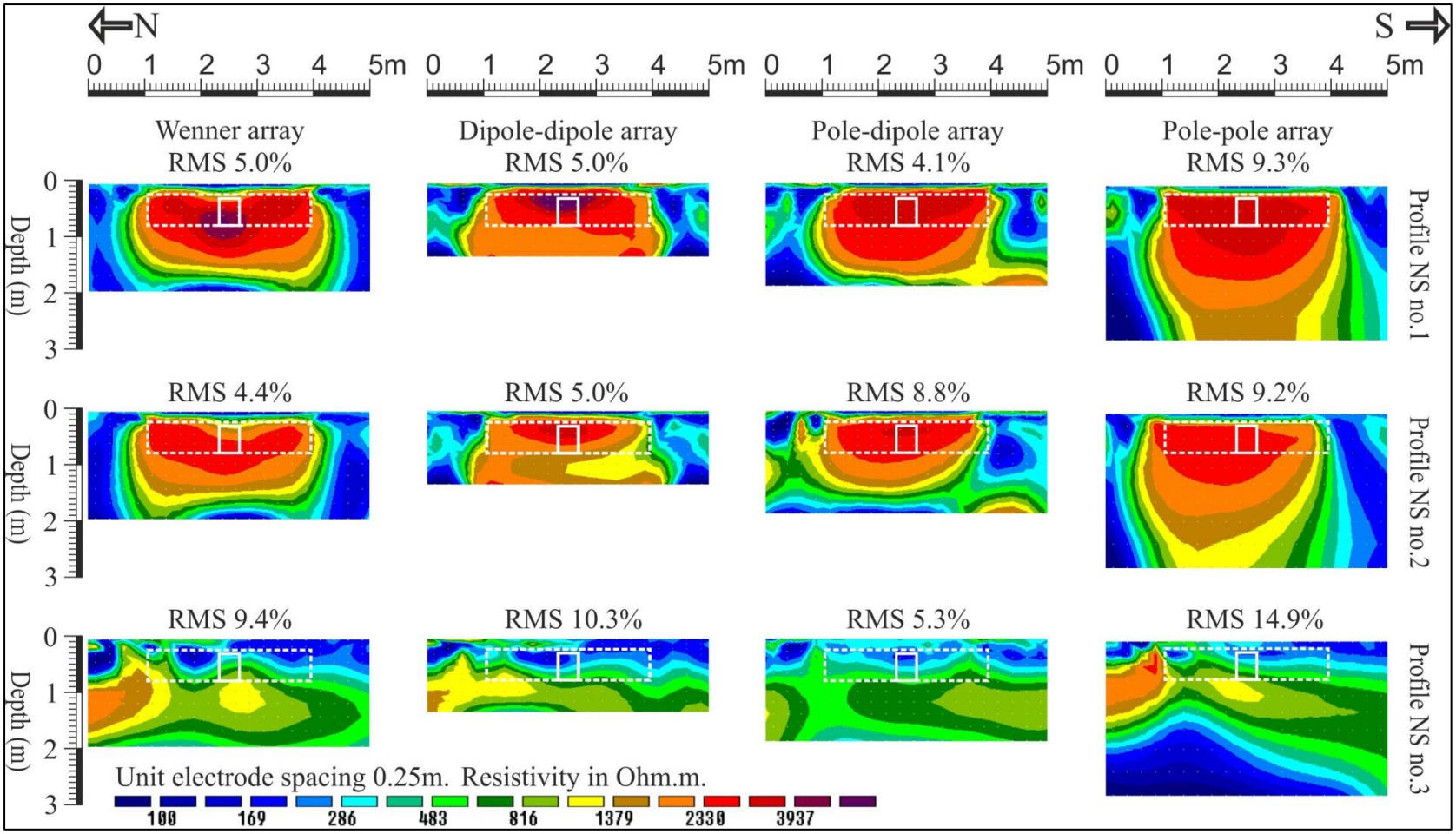

Figure 3: ERT 2D profile sections in N-S direction using least-square smoothness-constraint inversion with Wenner, dipole-dipole, pole-dipole, and pole-pole array configurations (see Fig.2 for location). White boxes indicate cleared wall foundation (solid line) and surrounding test site (dotted line) positions respectively. Pole-dipole data shown is merged from data collected in both directions on each profile. Inversion iteration 5 results shown throughout.

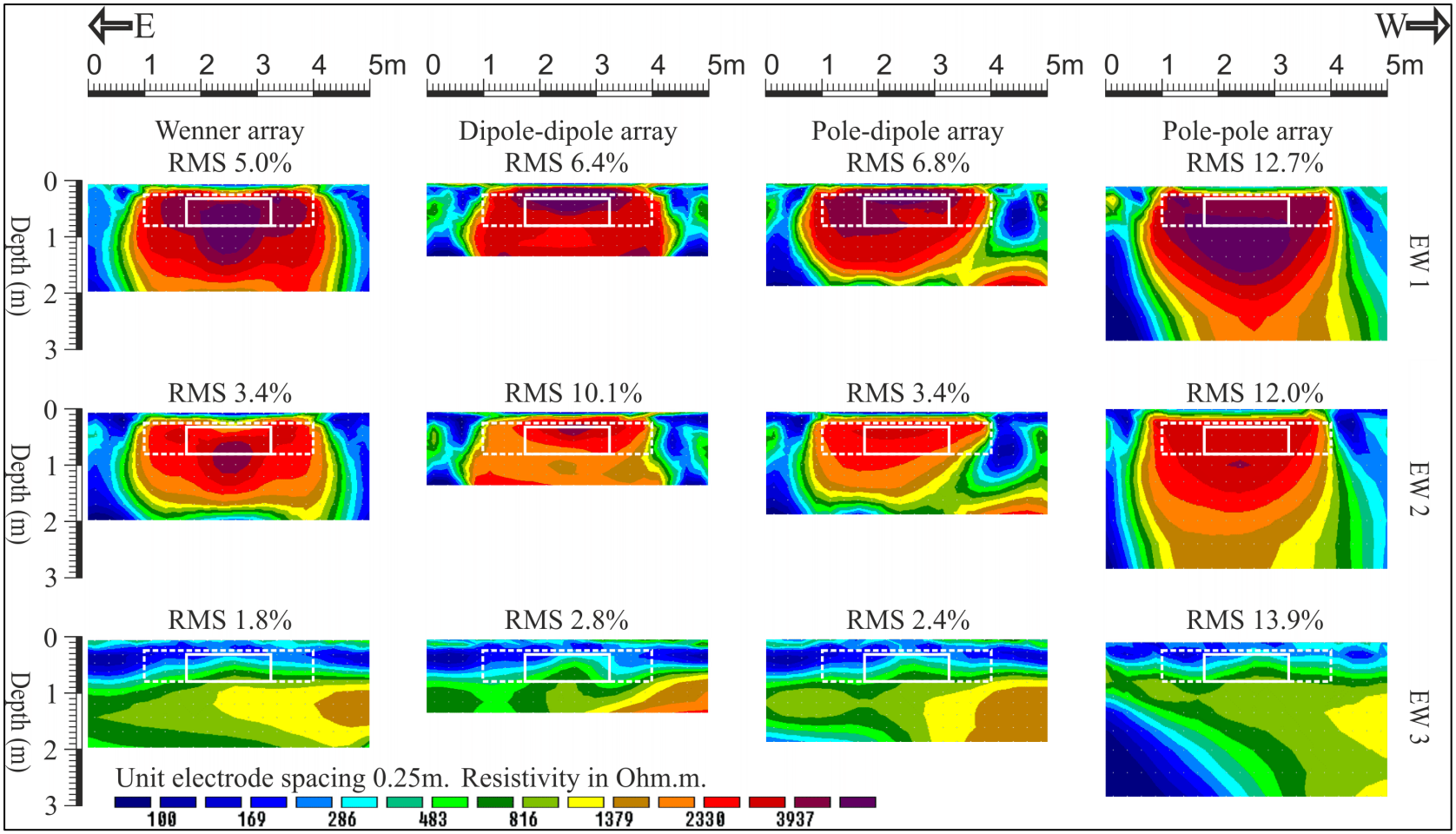

Figure 4: ERT 2D profile sections in E-W direction using least-square smoothness-constraint inversion with Wenner, dipole-dipole, pole-dipole, and pole-pole array configurations (see Fig. 2 for location). White boxes indicate cleared wall foundation (solid line) and surrounding test site (dotted line) positions respectively. Pole-dipole data shown is merged from data collected in both directions on each profile. Inversion iteration 5 results shown throughout.

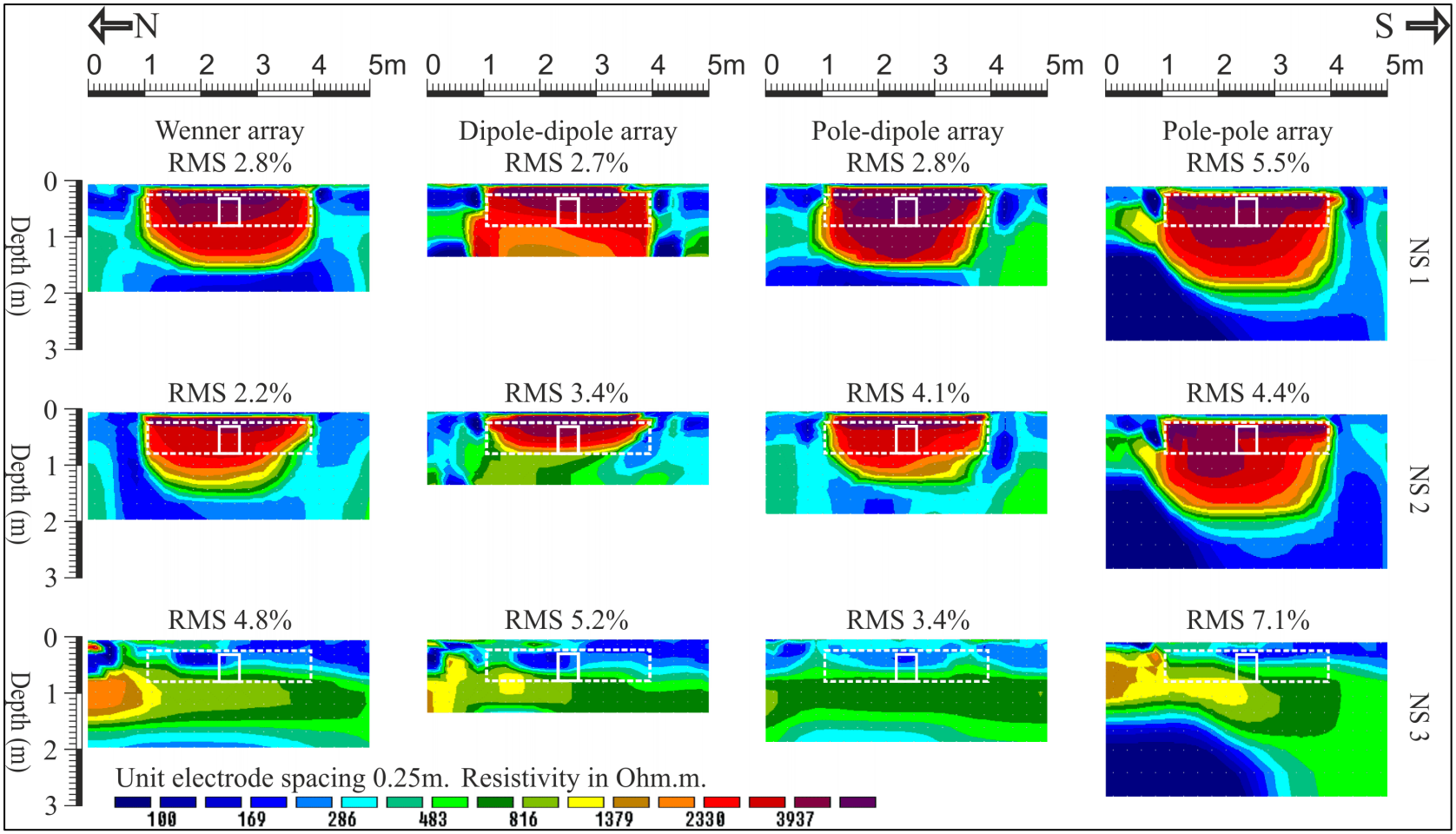

Figure 5: ERT 2D profile sections in N-S direction using robust inversion with Wenner, dipole-dipole, pole-dipole, and pole-pole array configurations (see Fig. 2 for location). White boxes indicate cleared wall foundation (solid line) and surrounding test site (dotted line) positions respectively. Pole-dipole data shown is merged from data collected in both directions on each profile. Inversion iteration 5 results shown throughout.

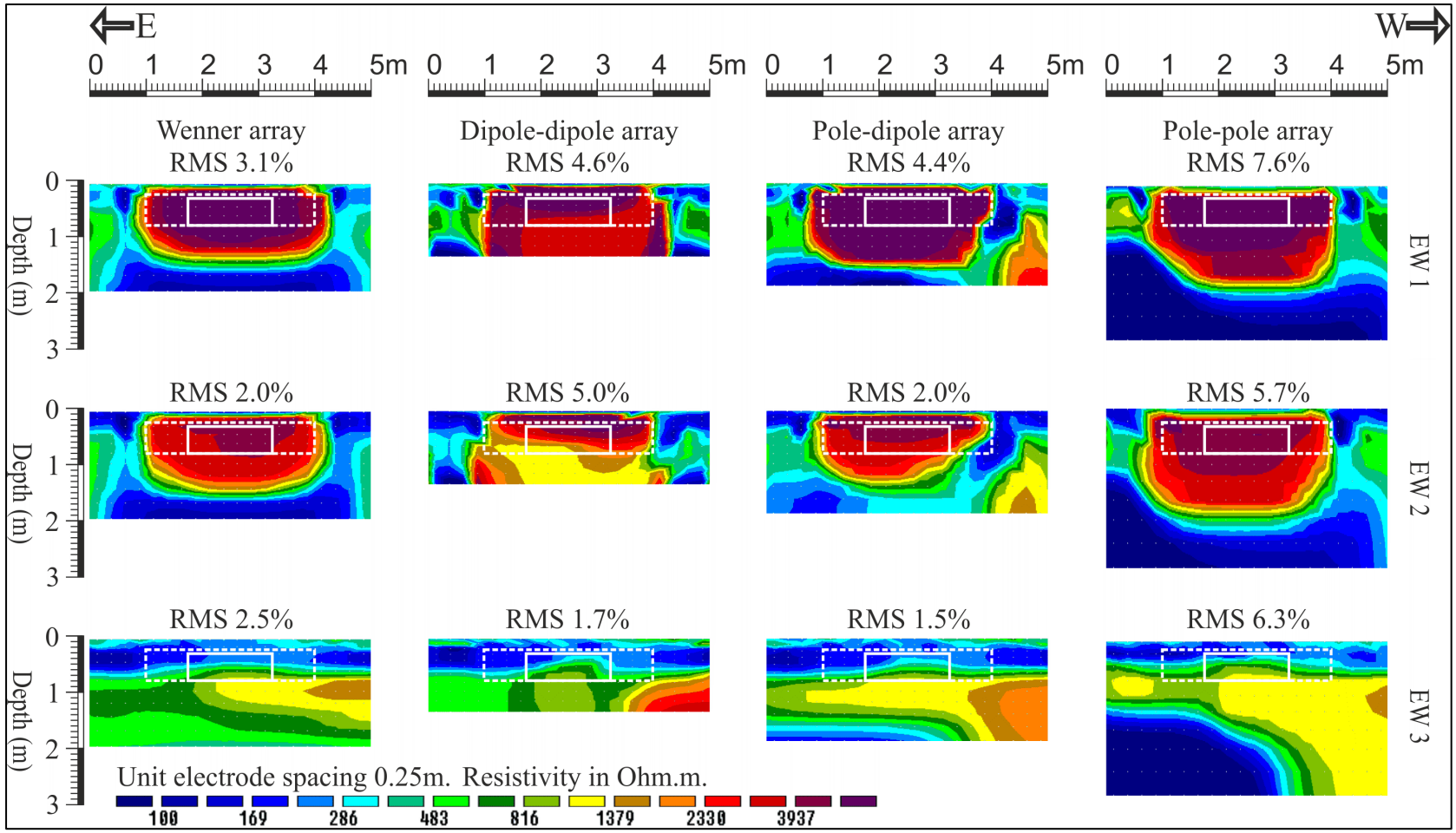

Figure 6: ERT 2D profile sections in E-W direction using robust inversion with Wenner, dipole-dipole, pole-dipole, and pole-pole array configurations (see Fig. 2 for location). White boxes indicate cleared wall foundation (solid line) and surrounding test site (dotted line) positions respectively. Pole-dipole data shown was merged from data collected in both directions on each profile. Inversion iteration 5 results shown throughout.

Based on the comparing the different electrode configurations, these 2D resistivity models were then qualitatively assessed based on two parameters: 1) the successful imaging of the cleared-brick wall foundation (i.e. which array could detect and discriminate the foundation from the gravel-fill) and, 2) the cleared-brick wall foundation accurate positioning (i.e. to what extent the brick wall position could be accurately located by the different array types). The assessment was ranked *Good* when the resistivity model (i.e. of a certain electrode configuration) achieved the two assessment parameters, *Moderate* when the model achieved one and ranked *Poor* when the model did not achieve either parameter. These were calculated for both the least-squares and robust inversion methods. Summary of these results are detailed in Table 2.

Table 2: ERT 2D profiles (both least-squares and robust inversions) were qualitatively assessed based on the accuracy of the cleared wall foundation position and being successfully imaged. Images were ranked **Good** for when the model achieved this, **Moderate** for when the model only achieved one and ranked **Poor** when the model did not achieve any parameters. Model RMS inversion percentages also included.

2D Profile number (see Fig.2) and array type	Least-square Inverted model, , RMS % error misfit	Cleared wall foundation well defined	Robust Inverted model, RMS % error misfit	Cleared wall foundation well defined
NS1, Wenner	5.0	Good	2.8	Moderate
NS1, Dipole-dipole	5.0	Good	2.7	Moderate
NS1, Pole-dipole	4.1	Poor	2.8	Poor
NS1, Pole-pole	9.3	Poor	5.5	Poor
NS2, Wenner	4.4	Moderate	2.2	Poor
NS2, Dipole-dipole	5.0	Moderate	3.4	Poor
NS2, Pole-dipole	8.8	Poor	4.1	Poor
NS2, Pole-pole	9.2	Poor	4.4	Poor
NS3, Wenner	9.4	N/A (off axis)	4.8	N/A (off axis)
NS3, Dipole-dipole	10.3	N/A (off axis)	5.2	N/A (off axis)
NS3, Pole-dipole	5.3	N/A (off axis)	3.4	N/A (off axis)
NS3, Pole-pole	14.9*	N/A (off axis)	7.1	N/A (off axis)
EW1, Wenner	5.0	Good	3.1	Moderate
EW1, Dipole-dipole	6.4	Good	4.6	Moderate
EW1, Pole-dipole	6.8	Moderate	4.4	Poor
EW1, Pole-pole	12.7*	Poor	7.6*	Poor
EW2, Wenner	3.4	Good	2.0	Moderate
EW2, Dipole-dipole	10.1	Good	5.0	Moderate
EW2, Pole-dipole	3.4	Moderate	2.0	Moderate

EW2, Pole-pole	12.0*	Poor	5.7	Poor
EW3, Wenner	1.8	N/A (off axis)	2.5	N/A (off axis)
EW3, Dipole-dipole	2.8	N/A (off axis)	1.7	N/A (off axis)
EW3, Pole-dipole	2.4	N/A (off axis)	1.5	N/A (off axis)
EW3, Pole-pole	13.9*	N/A (off axis)	6.3	N/A (off axis)

* indicated relatively high model errors.

For the least-squares inverted data profiles (Figs 3-4), the Wenner and dipole-dipole arrays generally gave *Good* results, whilst the pole-dipole and pole-pole array generally gave *Moderate* to *Poor* results (Table 2). Note that the wall foundation appeared to be spatially wider on EW profiles, when compared to the NS profiles (cf. Figs 3-4), as the EW profiles were orientated parallel to the buried target (Fig. 2).

For the robust inverted data profiles (Figs 5-6), the Wenner and dipole-dipole arrays generally gave *Moderate* results, whilst the pole-dipole and pole-pole arrays generally gave *Poor* results (Table 2). With these inversions, it was also harder to differentiate the cleared-brick wall foundation from the gravel-fill materials (cf. Fig. 5-6).

Discussion

This study has therefore investigated using electrical resistivity surveys to image a scaled model of a cleared-brick wall foundation, a common target for geotechnical geophysical surveys, especially in brownfield development sites (see Reynolds 2011). 2D ERT datasets were collected using the Wenner, dipole-dipole, pole-dipole and pole-pole array types, with data subsequently separately inverted during data processing using both least-squares and robust inversion algorithms. The resulting datasets found that the Wenner and dipole-dipole arrays generally located the position of the cleared-brick wall foundation, although not its base. The dipole-dipole configuration was more accurate, overall, than the Wenner for size/dimension of the target, which is surprising as most site investigations use the Wenner array (e.g. see Saad et al. 2010; Banham & Pringle 2011). The pole-pole array was generally the poorest in terms of target location and image quality.

The orientation of the 2D ERT profiles, in regards to the target location, was also found to be important, whilst all four arrays could detect the target in profiles parallel rather than only two detecting it in profiles perpendicular to the target, presumably as it was a larger target (1.5 m compared to 0.36 m respectively). Therefore, if the target orientation was not known in a site survey, multiple orientations of ERT 2D profiles should be collected to optimise survey results.

The study also illustrated the importance of minimum electrode spacing with regard to the target dimensions. Although the electrode spacing was a constant 0.25 m throughout all collected ERT survey profiles, the type of array significantly affected the respective survey array sensitivities. For example, the pole-pole array had a ~0.5x electrode spacing = 0.5 m minimum target size, the pole-dipole array had a ~1.6x electrode spacing = 0.4 m minimum target size, the dipole-dipole array had a ~1.8x electrode spacing = 0.45 m minimum target size and lastly the Wenner array had a ~1.7x electrode spacing = 0.425 m minimum target

size respectively – see Loke 2015). Thus this study finds that the array type is just as, if not more important than the electrode spacing to be optimal when designing electrical resistivity arrays. 2D ERT profiles will be sufficient to define a target where its approximate position is known, as Lysdahl et al. 2017 showed on coastal harbour foundations.

It would be preferable to quantify target anomaly contrasts with background materials, as others have undertaken in seismic surveys (see, for example, Guerriero et al. 2016; 2017).

Study limitations included the constrained nature of the test site surroundings (similar to those expected in urban brownfield sites) which limited survey profile lengths, and the strong contrast between the non-target gravel-fill and the background soils, which made it more difficult to resolve the target brick wall foundation. 3D surveys may have allowed unusual survey configurations to be collected, as Tejero-Andrade et al. (2015) illustrate, but this is unusual in commercial investigations of brownfield sites due to the extra time and associated costs incurred. Further work should collect 3D datasets, and vary the water content percentages in the surrounding pit to determine what effect these variations will have on target discrimination. Synthetic datasets could also be generated, varying the target body dimensions, depths below ground levels and other soil types to test these major variables.

Conclusions

Multiple ERT 2D profiles were collected over a controlled study site with a scaled model of a cleared-brick wall foundation, emplaced within a gravel-filled test site with a thin top soil. Wenner, dipole-dipole, pole-dipole and pole-pole configurations were trialled, before being separately inverted using both least-squares and robust inversion types. For the 2D resistivity surveys, the Wenner and dipole-dipole produced the best results, imaging the brick wall foundation, but not its base. Array type was deemed just as, or even more important than, electrode spacing when designing electrical resistivity surveys, due to different array type sensitivities to buried targets.

Acknowledgments

The Higher Committee for Education Development in Iraq (HCED) have provided funding for Raad Eissa's PhD. A 2003 SRIF2 UK Research Council award supported the geophysical equipment used during this research. EDINA Digimap is acknowledged for data retrieval support. Two anonymous reviewers greatly improved the manuscript for which the authors are grateful.

References

al Hagrey, S. A. and Petersen, T. 2011. Numerical and experimental mapping of small root zones using optimized surface and borehole resistivity tomography. *Geophysics*, **76**, G25-G35, https://dx.doi.org/10.1190/1.3545067.

Apuani, T, Giani, G.P., d'Attoli, M., Fischanger, F., Morelli, G., Ranieri, G., and Santarato, G. 2015. Assessment of the efficiency of consolidation treatment through injections of expanding resins by geotechnical tests and 3D electrical resistivity tomography. *The Scientific World Journal*, article ID 237930, 1-13, https://dx.doi.org/10.1155/2015/237930.

Arjwech, R., Everett, M.E., Briaud, J.L., Hurlebaus, S., Medina-Cetina, Z., Truker, S. and Yousefpour, N. 2013. Electrical resistivity imaging of unknown bridge foundations. *Near Surface Geophysics*, **11**, 591-598, https://dx.doi.org/10.3997/1873-0604.2013023.

Banham, S.G. and Pringle, J.K. 2011. Geophysical and intrusive site investigations to detect an abandoned coal-mine access shaft, Apedale, Staffordshire, UK. *Near Surface Geophysics*, **9**, 483-496, https://dx.doi.org/10.3997/1873-0604.2011028.

Bentley, L.R. and Gharibi, M. 2004. Two- and three-dimensional electrical resistivity imaging at a heterogeneous remediation site. *Geophysics*, **69**, 674–680, https://dx.doi.org/10.1190/1.1759453.

Cardarelli, E., Donno, G., Oliveti, I. and Scatigno, C. 2018. Three-dimensional reconstruction of a masonry building through electrical and seismic tomography validated by biological analyses. Near Surface Geophysics, **16**, 53-65, https://dx.doi.org/10.3997/1873-0604.2017040.

317 Cardarelli, E., Cercato, M., Cerreto, A. and Di Filippo, G. 2010. Electrical resistivity and
318 seismic refraction tomography to detect buried cavities. *Geophysical Prospecting*, **58**, 685-
319 695, https://dx.doi.org/10.1111/j.1365-2478.2009.00854.x.

320 Cardarelli, E., Cercato, M. and Di Filippo, G. 2007. Assessing foundation stability and soil-
321 structure interaction through integrated geophysical techniques: a case history in Rome
322 (Italy). *Near Surface Geophysics*, **5**, 141–147, https://dx.doi.org/10.3997/1873-
323 0604.2006026

324 Cassidy, N. 2001. *The application of mathematical modelling in the interpretation of near-*
325 *surface archaeological ground-penetration radar.* Ph.D. thesis, Keele University.

326 Chambers, J.E., Wilkinson, P.B., Weller, A.L., Meldrum, P.I., Ogilvy, R.D. and Caunt, S.
327 2007. Mineshaft imaging using surface and crosshole 3D electrical resistivity tomography:
328 A case study history from the East Pennine Coalfield, UK. *Journal of Applied Geophysics*,
329 **62**, 324-337, https://dx.doi.org/10.1016/j.jappgeo.2007.03.004.

330 Chrétien, M., Lataste, J.F., Fabre, R. and Denis, A. 2014. Electrical resistivity tomography to
331 understand clay behaviour during seasonal water content variations. *Engineering Geology*,
332 **169**, 112-123, https://dx.doi.org/10.1016/j.enggeo.2013.11.019.

333 Cosenza, P., Marmet, E., Rejiba, F., Cui, Y., Tabbagh, A. and Charlery, Y. 2006.
334 Correlations between geotechnical and electrical data: a case study at Garchy in France.
335 *Journal of Applied Geophysics*, **60**, 165–178,
336 https://dx.doi.org/10.1016/j.jappgeo.2006.02.003.

337 Dahlin, T. 2001. The development of DC resistivity imaging techniques. *Computers &*
338 *Geosciences*, **27**, 1019-1029, https://dx.doi.org/10.1016/S0098-3004(00)00160-6.

339 Dahlin, T. and Zhou, B. 2004. A numerical comparison of 2D resistivity imaging with 10
340 electrode arrays. *Geophysical prospecting*, **52**, 379-398,
341 https://dx.doi.org/10.1111/j.1365-2478.2004.00423.x.

342 Deceuster, J., Delgranche, J., Kaufmann, O. and 2006. 2D cross-borehole resistivity
343 tomographies below foundations as a tool to design proper remedial actions in covered
344 karst. *Journal of Applied Geophysics*, **60** (1), 68–86,
345 https://dx.doi.org/10.1016/j.jappgeo.2005.12.005.

346 Donohue, S., Gavin, K. and Tolooiyan, A. 2011. Geophysical and geotechnical assessment of
347 a railway embankment failure. *Near Surface Geophysics*, **9** (1), 33–44,
348 https://dx.doi.org/10.3997/1873-0604.2010040.

349 Edwards, L.S. 1977. A modified pseudosection for resistivity and induced-polarization.
350 *Geophysics*, **42** (5), 1020-1036, https://dx.doi.org/10.1190/1.1440762.

351 Fischanger, F., Morelli, G., Ranieri, G., Santarato, G., and Occhi, M. 2013. 4D cross-
352 borehole electrical resistivity tomography to control resin injection for ground stabilization:
353 a case study history in Venice (Italy). *Near Surface Geophysics*, (11), 41-50,
354 https://dx.doi.org/10.3997/1873-0604.2012056.

355 Gaffney, C., Harris, C., Pope-Carter, F., Bonsall, J., Fry, R. And Parkyn, A. 2015. Still
356 searching for graves: an analytical strategy for interpreting geophysical data used in the
357 search for "unmarked" graves. *Near Surface Geophysics*, **13**, 557-569,
358 https://dx.doi.org/10.3997/1873-0604.2015029.

359 Gaffney, C. 2008. Detecting trend in the prediction of the buried past: a review of
360 geophysical techniques in archaeology. *Archaeometry*, **50**, 313-336,
361 https://dx.doi.org/10.1111/j.1475-4754.2008.00388.x.

362 Garman, K. and Purcell, S. 2004. Three-dimensional electrical resistivity surveys to identify
363 buried karst features affecting road projects, subsurface evaluation, Inc. [Available
364 online]:http//www.dot.state.fl.us/statematerialsoffice/geotechnical/conference/materials//g
365 arman-pursel.pdf. [Accessed 09/02/2016].

366 Guerriero, L. Bertello, L., Cadozo, N., Berti, M., Grelle, G., Revellino, P. 2017. Unsteady
367 sediment discharge in earth flows: A case study from the Mount Pizzuto earth flow,
368 southern Italy. *Geomorphology*, **295**, 260-284.
369 https://dx.doi.org/10.1016/j.geomorph.2017.07.011

370 Guerriero, L., Coe, J.A., Revellio, P., Grelle, G., Pinto, F., Guadagno, F. 2016. Influence of
371 slip-surface geometry on earth-flow deformation, Montaguto earth flow, southern Italy,
372 *Geomorphology*, **219**, 285-305. https://dx.doi.org/10.1016/j.geomorph.2014.04.039

373 Gunn. A.D., Chambers, J.E., Uhlemann, S., Wilkinson, P.B., Meldrum, P.I., Dijkstra, T.D.,
374 Haslam, E., Kirkham, M., Wragg, J., Holyoake, S., Hughes, P.N, Hen-Jones, R. and
375 Glendinning, S. 2015. Moisture monitoring in clay embankments using electrical
376 resistivity tomography. *Construction and Building Materials*, **92**, 82-94,
377 http://dx.doi.org/10.1016/j.conbuildmat.2014.06.007.

378 Juerges, A., Pringle, J.K., Jervis, J.R. and Masters, P. (2010). Comparisons of magnetic and
379 electrical resistivity surveys over simulated clandestine graves in contrasting burial
380 environments. *Near Surface Geophysics*, **8**, 529-539, https://dx.doi.org/10.3997/1873-
381 0604.2010041.

382 Kampke, A. 1999. Focused imaging of electrical resistivity data in archaeological prospecting.
383 *Journal of Applied Geophysics*, **41**, 215-227, https://dx.doi.org/10.1016/S0926-
384 9851(98)00043-3.

385 Keary, P., Brooks, M. and Hill, I. 2002. *Introduction to Geophysical Exploration*. 3rd edition.
386 The United Kingdom: Blackwell publishing, **262**.

387 Loke, M.H., Wilkinson, P.B. and Chambers, J.E. 2010. Parallel computing of optimized
388 arrays for 2-D electrical imaging surveys. *Geophysical Journal International*, **183**, 1302-
389 1315, https://dx.doi.org/10.1111/j.1365-246X.2010.04796.x.

390 Loke, M.H. and Barker, R. D. 1995. Least-square deconvolution of apparent resistivity
391 pseudosections. *Geophysics*, **60** (6), 1682-1690, https://dx.doi.org/10.1190/1.1443900.

392 Loke M.H. and Barker R.D. 1996. Rapid least-squares inversion of apparent resistivity
393 pseudosections using a quasi-Newton method. *Geophysical Prospection*, **44**, 131–152,
394 https://dx.doi.org/10.1111/j.1365-2478.1996.tb00142.x.

395 Loke M.H., Acworth I. and Dahlin T. 2003. A comparison of smooth and blocky inversion
396 methods in 2D electrical imaging surveys. *Exploration Geophysics*, **34**, 182–187,
397 https://dx.doi.org/10.1071/EG03182.

398 Loke, M.H. 2015. Tutorial 2-D and 3-D electrical imaging survey. [Available online]:
399 www.geotomosoft.com/downloads.php. Accessed September 2015.

400 Loke, M.H., and Dahlin, T. 2002. A comparison of the Gauss–Newton and quasi-Newton
401 methods in resistivity imaging inversion. *Journal of Applied Geophysics*, **49**, 149–162,
402 https://dx.doi.org/10.1016/S0926-9851(01)00106-9.

403 Loke, M.H., Chambers, J., Rucker, D.F., Wilkinson, P.B. 2013. Recent developments in the
404 direct-current geoelectrical imaging method. *Journal of Applied Geophysics*, **95**, 135-156,
405 https://dx.doi.org/10.1016/j.jappgeo.2013.02.017.

406 Loke, M.H., Wilkinson, P.B., Chambers, J.E. 2010. Fast computation of optimized electrode
407 arrays for 2D resistivity surveys. *Computers & Geosciences*, **36**, 1414-1426,
408 https://dx.doi.org/10.1016/j.cageo.2010.03.016.

409 Lysdahl, A.K., Bazin, S., Christensen, C., Ahrens, S., Günther, T. and Pfaffhuber, A. 2017.
410 Comparison between 2D and 3D ERT inversion for engineering site investigation – a case
411 study from Oslo Harbour. *Near Surface Geophysics*, **15**, 201-209,
412 https://dx.doi.org/10.3997/1873-0604.2016052.

413 Long, M., Pfaffhuber, A.A., Bazin, S., Kåsin, K., Gylland, A. and Montaflia, A. 2017.
414 Glacio-marine clay resistivity as a proxy for remoulded shear strength: correlations and
415 limitations. *Quarterly Journal of Engineering Geology and Hydrogeology*, **51**, 63-78,
416 https://dx.doi.org/10.1144/qjegh2016-136.

417 Cuthbert, M.O., Mackay, R., Tellam, J.H. and Barker , R.D. 2009. The use of electrical
418 resistivity tomography in deriving local-scale models of recharge through superficial
419 deposits. Quarterly Journal of Engineering Geology and Hydrogeology, 42, 199-209,
420 https://dx.doi.org/10.1144/1470-9236/08-023.

421 Maurer, H., Curtis, A. and Boerner, D.E. 2010. Recent advances in optimized geophysical
422 survey design. *Geophysics*, **75**, A177-A194, https://dx.doi.org/10.1190/1.3484194.

423 Nyquist, J.E. and Roth, M.J.S. 2005. Improved 3D pole-dipole resistivity surveys using radial
424 measurement pairs. *Geophysics Research Letters*, **32**, L21416, 4,
425 https://dx.doi.org/10.1029/2005GL024153.

426 Orfanos, C. and Apostolopoulos. G. 2011. 2D-3D resistivity and microgravity measurements
427 for the detection of an ancient tunnel in the Lavrion area, Greece. *Near Surface*
428 *Geophysics*, **9**, 449-457, https://dx.doi.org/10.3997/1873-0604.2011024.

Reynolds, J.M. 2011. *Introduction to Applied and Environmental Geophysics*. 2nd ed edition. John Wiley & Sons, 696.

Saad, R., Nawawi, M.N.M., Muztaza, N.M. and Jusoh, Z. 2010. *Testing of resistivity imaging method with different protocols to detect void using miniature model. In; progress of physics research in Malaysia: PERFIK2009*, **1250** (1), 177-180.

Soupios, P.M., Georgakopoulos, P, Papadopoulos, N., Saltas, V., Andreadakis, A., Vallianatos, F., Sarris, A. and Makris, J.P. 2007. Use of engineering geophysics to investigate a site for a building foundation. *Journal of Geophysics and Engineering*, **4**, 94–103, https://dx.doi.org/10.1088/1742-2132/4/1/011.

Stummer, P., Maurer, H. and Green, A.G. 2004. Experimental design: Electrical resistivity data sets that provide optimum subsurface information. *Geophysics*, **69**, 120-139, https://dx.doi.org/10.1190/1.1649381.

Szalai, S. and Szarka, L. 2008. On the classification of surface geoelectric arrays. *Geophysical Prospection*, **56**, 159-175, https://dx.doi.org/10.1111/j.1365-2478.2007.00673.x.

Tejero-Andrade, A., Cifuentes, G., Chavez, R.E., Lopez-Gonzalez, A.E. and Delgado-Solorzano, C. 2015. L- and CORNER-arrays for 3D electric resistivity tomography: an alternative for geophysical surveys in urban zones. *Near Surface Geophysics*, **13**, 355-367, https://dx.doi.org/10.3997/1873-0604.2015015.

Wilkinson, P.B., Meldrum, P.I., Chambers, J.E., Kuras, O. and Ogilvy, R.D. 2006. Improved strategies for the automatic selection of optimized sets of electrical resistivity tomography measurement configurations. *Geophysical Journal International*, **167**, 1119-1126, https://dx.doi.org/10.1111/j.1365-246X.2006.03196.x.

452 Wilkinson, P.B., Loke, M.H., Meldrum, P.I., Chambers, J.E., Kuras, O., Gunn, D.A. and
453 Ogilvy, R. D. 2012. Practical aspects of applied optimized survey design for electrical
454 resistivity tomography. *Geophysical Journal International*, **189**, 428-440,
455 https://dx.doi.org/10.1111/j.1365-246X.2012.05372.x.

456 Zhu, J., Currens, J.C., Dinger, J.S. and 2011. Challenges of using electrical resistivity method
457 to locate karst conduits-a field case in the Inner Bluegrass Region, Kentucky. *Journal of*
458 *Applied Geophysics*, **75** (3), 523–530, ttps://dx.doi.org/doi:10.1016/j.jappgeo.2011.08.009.

459 Zhu, T., Zhou, J. and Wang, H. 2017. Localization and characterization of the Zhandian-
460 Renhe fault zone in Zibo city, Shandong province, China, using electrical resistivity
461 tomography (ERT). *Journal of Applied Geophysics*, **136**, 343-352,
462 http://dx.doi.org/10.1016/j.jappgeo.2016.11.016.